INTERNATIONAL JOURNAL FOR NUMERICAL METHODS IN FLUIDS
Int. J. Numer. Meth. Fluids 2000; **00**:1–6 *Prepared using* fldauth.cls *[Version: 2002/09/18 v1.01]*

Stabilized finite element method based on local preconditioning for unsteady compressible flows in deformable domains with emphasis on the low Mach number limit application

Ezequiel J. López*†, Norberto M. Nigro, Sofía S. Sarraf and Santiago Márquez Damián

Centro Internacional de Métodos Computacionales en Ingeniería (CIMEC), INTEC-CONICET-UNL, Güemes 3450, 3000 Santa Fe, ARGENTINA

SUMMARY

Flows with low Mach numbers represent a limit situation in the solution of compressible flows. As the Mach number tends to zero, compressible flow solvers suffer severe deficiencies, both in efficiency and accuracy. The preconditioning of flow equations is one of the approaches actually proposed to capture the solution in the low Mach number limit. In this method, the time derivatives are premultiplied by a suitable preconditioning matrix in order to achieve a well-conditioned system by means of the scaling of the system eigenvalues. Hence, the modified equations have only steady-state solutions in common with the original system. For the application of these methods to unsteady problems, the dual-time-stepping technique has emerged, where the physical time derivative terms are treated as source and/or reactive terms. In this work, we show that a preconditioning matrix defined to compute steady-state solutions may not be a good election for unsteady problems. The application of a 'steady-state' preconditioning matrix to unsteady problems with an ALE (Arbitrary Lagrangian Eulerian) approach is presented. The equations are discretized in space using a stabilized Finite Element method and in time using finite differences. Also the treatment of dynamic boundary conditions for the preconditioned system is discussed. Several test cases are solved, including incompressible flows and the in-cylinder flow in an opposed-piston engine under cold conditions.

KEY WORDS: Low Mach number compressible viscous flows; Local preconditioning; Arbitrary Lagrangian Eulerian, Stabilized Finite Elements

1. INTRODUCTION

The low Mach number (M) setting is a singular limiting situation in compressible flows. When the Mach number approaches to zero, the strategies based on density to solve the flow equations suffer severe deficiencies, both in efficiency and accuracy. This fact occurs since in the low Mach number limit the system of equations is ill-conditioned, with a condition

*Correspondence to: Ezequiel J. López, Centro Internacional de Métodos Computacionales en Ingeniería (CIMEC), INTEC-CONICET-UNL, Güemes 3450, 3000 Santa Fe, ARGENTINA
†E-mail: ejlopez@santafe-conicet.gov.ar

Received 3 November 2009
Revised

number $\mathcal{O}(1/M)$ in the inviscid case [1]. There are two main approaches to circumvent this drawback: firstly, the modification of compressible solvers (density-based) downward to low Mach numbers [1, 2, 3, 4, 5, 6]; secondly, extending incompressible solvers (pressure-based) towards the compressible regime [7, 8, 9]. Also there are unified formulations, as the method proposed by Mittal and Tezduyar [10].

For density-based methods, two different techniques have been proposed to capture solution convergence for low-Mach number regimes: preconditioning and asymptotic methods. Both techniques achieve rescaling of the system condition number. The asymptotic method introduces a perturbed form of the equations discarding specific terms, so that the physical acoustic waves are replaced by pseudo-acoustic modes. The magnitude of the propagation speeds of these pseudo-acoustic modes is similar to the fluid velocity [11]. Although perturbation procedures are highly robust and applicable to both viscous and inviscid flows, the nature of the perturbation limits their usage, particularly with respect to mixed compressible-incompressible flows.

Preconditioning schemes consist in premultiplying time derivatives by a suitable preconditioning matrix. This scales the eigenvalues of the system to similar magnitude orders and removes the disparity in wave-speeds, leading to a well-conditioned system [1, 3, 15]. The modified equations have only steady-state solutions in common with the original system (hence, are devoid of true transients). For the application of these methods to unsteady problems the dual-time-stepping technique has emerged, where the physical time derivative terms are treated as source and/or reactive terms. During each physical time step, the system of pseudo-temporal equations is advanced in artificial time until reaching a pseudo-steady-state [12, 13, 14, 5, 6]. Several local preconditioning matrices have been designed for steady state problems, with very good results [1, 2, 3]. However, recent works have shown that these preconditioning matrices may not be appropriate for unsteady flows [5].

The proposal in this work is to apply the method of preconditioning due to its ability to work in a wide range of Mach and Reynolds numbers [16]. This method is used in conjunction with the dual-time-stepping technique in order to deal with transient problems. The governing equations are discretized in space and time using a stabilized Finite Element Method (FEM) and finite differences, respectively. Because the preconditioning modifies the wave-speeds, the FEM stabilization should be computed properly for this situation. The preconditioning matrix applied here was proposed by Choi and Merkle [3] to solve steady compressible flows using the Finite Volume method. Nigro *et al.* [17, 16] applied this preconditioning matrix to formulate a stabilized FEM scheme able to solve steady compressible flow problems.

The eigenvalues of the Navier-Stokes equation system for unsteady compressible flow with an ALE (Arbitrary Lagrangian Eulerian) formulation are computed. Based on the maximum to minimum eigenvalues ratio, we analyze some definitions of the adjustable coefficients in the preconditioning matrix. We present a proposal for the computation of the stabilization term for the FEM technique and, in addition, the treatment of absorbing boundary conditions. Several test cases are included. Some of them are incompressible flows, and thus compared with solutions of the incompressible Navier-Stokes equations.

2. PROBLEM DEFINITION AND EIGENVALUES ANALYSIS

Let $\Omega \subset \mathbb{R}^{n_\mathrm{d}}$ the spatial domain and $(0, t_\mathrm{f})$ the temporal domain, where n_d is the number of space dimensions, and let Γ the boundary of Ω. The spatial and temporal coordinates are denoted by $\mathbf{x} = [x_1, \ldots, x_{n_\mathrm{d}}]^T$ and t, respectively. The Navier-Stokes equations governing a compressible viscous flow, expressed in the quasi-linear form can be written as [18]

$$\frac{\partial \mathbf{U}}{\partial t} + \mathbf{A}_i \frac{\partial \mathbf{U}}{\partial x_i} = \frac{\partial}{\partial x_i}\left(\mathbf{K}_{ij}\frac{\partial \mathbf{U}}{\partial x_j}\right) + \mathbf{S} \quad \text{on } \Omega \times (0, t_\mathrm{f}) \tag{1}$$

$\mathbf{U} = [\rho, \rho\mathbf{u}, \rho e]^T$ being the *conservative variables* vector, where the symbols ρ, $\mathbf{u}$, p and e represent the density, velocity, pressure and total specific energy, respectively. $\mathbf{A}_i$ is the advective jacobian matrix, $\mathbf{K}_{ij}$ is the diffusivity matrix and $\mathbf{S}$ is the source vector. The system of equations is closed once the pressure is related to the problem variables through the equation of state, $p = (\gamma - 1)\rho(e - \|\mathbf{u}\|^2/2)$, where $\|\cdot\|$ is the standard euclidean norm for vectors and γ is the ratio of specific heats which is assumed to be constant.

Since in the low Mach number limit the density tends to be constant in space, it is convenient to perform the analysis using the *viscous variables* defined as

$$\mathbf{Q} = [p, \mathbf{u}, T]^T \tag{2}$$

where T is the fluid temperature.

The idea in the preconditioning method is to premultiply the time derivatives by a properly defined matrix in order to scale the eigenvalues of the equation system to similar magnitude orders. The method modifies the transient evolution of the flow and, thus, it is only applicable to steady state simulations. In order to apply the preconditioning strategy to unsteady problems, the dual-time-stepping technique has emerged [12, 13]. In this technique, two times must be considered: the physical time and the *pseudo-time* τ. The solution is obtained adding a preconditioned pseudo-time derivative to equation (1). At each physical time step, the system is solved until the pseudo-steady state is reached when $\tau \to \infty$. Let $\mathbf{\Gamma}$ denotes the preconditioning matrix, then the system of equations modified by the dual-time-stepping strategy is written as [14]

$$\mathbf{\Gamma}\frac{\partial \mathbf{U}}{\partial \tau} + \frac{\partial \mathbf{U}}{\partial t} + \mathbf{A}_i \frac{\partial \mathbf{U}}{\partial x_i} = \frac{\partial}{\partial x_i}\left(\mathbf{K}_{ij}\frac{\partial \mathbf{U}}{\partial x_j}\right) + \mathbf{S} \tag{3}$$

In the viscous variables basis, equation (3) is expressed as

$$\mathbf{\Gamma}\frac{\partial \mathbf{U}}{\partial \mathbf{Q}}\frac{\partial \mathbf{Q}}{\partial \tau} + \frac{\partial \mathbf{U}}{\partial \mathbf{Q}}\frac{\partial \mathbf{Q}}{\partial t} + \mathbf{A}_i \frac{\partial \mathbf{U}}{\partial \mathbf{Q}}\frac{\partial \mathbf{Q}}{\partial x_i} = \frac{\partial}{\partial x_i}\left(\mathbf{K}_{ij}\frac{\partial \mathbf{U}}{\partial \mathbf{Q}}\frac{\partial \mathbf{Q}}{\partial x_j}\right) + \mathbf{S} \tag{4}$$

Let

$$\mathbf{\Gamma}_\mathrm{v} = \mathbf{\Gamma}\frac{\partial \mathbf{U}}{\partial \mathbf{Q}} \tag{5}$$

the preconditioning matrix in the viscous variables basis. Hence, after premultiplying equation (4) by the inverse matrix $\mathbf{\Gamma}_\mathrm{v}^{-1}$, the following expression is obtained

$$\frac{\partial \mathbf{Q}}{\partial \tau} + \mathbf{\Gamma}_\mathrm{v}^{-1}\frac{\partial \mathbf{U}}{\partial \mathbf{Q}}\frac{\partial \mathbf{Q}}{\partial t} + \mathbf{\Gamma}_\mathrm{v}^{-1}\mathbf{A}_i \frac{\partial \mathbf{U}}{\partial \mathbf{Q}}\frac{\partial \mathbf{Q}}{\partial x_i} = \mathbf{\Gamma}_\mathrm{v}^{-1}\frac{\partial}{\partial x_i}\left(\mathbf{K}_{ij}\frac{\partial \mathbf{U}}{\partial \mathbf{Q}}\frac{\partial \mathbf{Q}}{\partial x_j}\right) + \mathbf{\Gamma}_\mathrm{v}^{-1}\mathbf{S} \tag{6}$$

In this work, the analysis is done using the preconditioning matrix proposed by Choi and Merkle [3] for the resolution of steady state problems in the low Mach number limit. In the **Q** variables basis this preconditioning matrix takes the following form for the 3D case

$$\mathbf{\Gamma}_{\mathrm{v}} = \begin{bmatrix} \dfrac{1}{\beta M_{\mathrm{r}}^2} & 0 & 0 & 0 & 0 \\ \dfrac{u_1}{\beta M_{\mathrm{r}}^2} & \rho & 0 & 0 & 0 \\ \dfrac{u_2}{\beta M_{\mathrm{r}}^2} & 0 & \rho & 0 & 0 \\ \dfrac{u_3}{\beta M_{\mathrm{r}}^2} & 0 & 0 & \rho & 0 \\ \dfrac{\rho e + p}{\rho \beta M_{\mathrm{r}}^2} - \delta & \rho u_1 & \rho u_2 & \rho u_3 & \dfrac{\gamma \rho R}{\gamma - 1} \end{bmatrix} \tag{7}$$

where M_{r} is a reference Mach number, u_i, $i = 1, 2, 3$ are the components of the fluid velocity, R is the particular gas constant, δ is a constant that plays the role of a coefficient of the time derivative of pressure in the energy equation and $\beta = zc^2$, $c = \sqrt{\gamma RT}$ being the sound speed and $z = \max(1, z_{\mathrm{vis}})$, with

$$z_{\mathrm{vis}} = \frac{\alpha(\alpha - 1)}{M_{\mathrm{r}}^2[\alpha - 1 + c^2/(\mathbf{u} \cdot \mathbf{s})^2]}$$
$$\alpha = \frac{C\tilde{F}L}{\tilde{\sigma} Re_h}$$

In the last equation $C\tilde{F}L$ and $\tilde{\sigma}$ are, respectively, the Courant-Friedrichs-Levy and the von Neumann numbers for the preconditioned system based on pseudo-time discretization parameters [†], $Re_h = \rho \|\mathbf{u}\| h/\mu$ is the cell Reynolds number based on the characteristic element length h, and $\mathbf{s}$ is the unit vector aligned with the flow velocity. In the next section we will discuss the choice of M_{r} (see equation (22) for the original definition given by Choi and Merkle). According to Choi and Merkle, there are two convenient choices of the δ parameter: 0 or 1. In this study, $\delta = 1$ is used. With this preconditioning matrix, the preconditioned equations are nearly identical to the equations obtained when the method of artificial compressibility is applied, with the addition of the equation of energy conservation [3].

In order to study the eigenvalues of the preconditioned equation system, we Fourier transform the equation (6) after discretizing the physical time derivative term. Let

$$\begin{aligned} \tilde{\mathbf{A}}_{\mathrm{v},\,i} &= \mathbf{\Gamma}_{\mathrm{v}}^{-1} \mathbf{A}_i \frac{\partial \mathbf{U}}{\partial \mathbf{Q}} \\ \tilde{\mathbf{K}}_{\mathrm{v},\,ij} &= \mathbf{\Gamma}_{\mathrm{v}}^{-1} \mathbf{K}_{ij} \frac{\partial \mathbf{U}}{\partial \mathbf{Q}} \\ \tilde{\mathbf{S}}_{\mathrm{v}} &= \mathbf{\Gamma}_{\mathrm{v}}^{-1} \mathbf{S} \end{aligned} \tag{8}$$

The discretization of the physical time derivative is done using Backward Differentiation

[†] $C\tilde{F}L = \max_i(\lambda_i)\Delta\tau/h$, where λ_i represents the wave propagation speed and $\Delta\tau$ is the pseudo-time step. $\tilde{\sigma} = \mu\Delta\tau/\rho h^2$, where μ is the dynamic viscosity of the fluid.

Formulas (BDFs)

$$\frac{\partial \mathbf{Q}}{\partial t} \approx \frac{c_{k0}\mathbf{Q}^{n+1} - E(\mathbf{Q}^n, \mathbf{Q}^{n-1}, \dots)}{\Delta t}, \tag{9}$$

where $E = \sum_{j=1}^{k} c_{kj}\mathbf{Q}^{n-j+1}$, c_{kj}, $j = 0, \dots, k$ are constants that depend on the temporal order of the scheme (k) and Δt is the time step. Discretizing the time derivative, the system of equations (6) can be written as

$$\frac{\partial \mathbf{Q}}{\partial \tau} + \frac{c_{k0}}{\Delta t}\boldsymbol{\Gamma}_{\mathrm{v}}^{-1}\frac{\partial \mathbf{U}}{\partial \mathbf{Q}}\mathbf{Q} + \tilde{\mathbf{A}}_{\mathrm{v},\,i}\frac{\partial \mathbf{Q}}{\partial x_i} = \frac{\partial}{\partial x_i}\left(\tilde{\mathbf{K}}_{\mathrm{v},\,ij}\frac{\partial \mathbf{Q}}{\partial x_j}\right) + \tilde{\mathbf{S}}_{\mathrm{v}} + \frac{1}{\Delta t}\boldsymbol{\Gamma}_{\mathrm{v}}^{-1}\frac{\partial \mathbf{U}}{\partial \mathbf{Q}}E(\mathbf{Q}^n, \mathbf{Q}^{n-1}, \dots) \tag{10}$$

In order to simplify the notation, the index $n+1$ for the variables evaluated at the current time was dropped from equation (10).

With the aim of finding analytical expressions for the eigenvalues of the preconditioned system of equations we neglect (by the time) the diffusive and source terms in equation (10), which leads to the following expression

$$\frac{\partial \mathbf{Q}}{\partial \tau} + \frac{c_{k0}}{\Delta t}\boldsymbol{\Gamma}_{\mathrm{v}}^{-1}\frac{\partial \mathbf{U}}{\partial \mathbf{Q}}\mathbf{Q} + \tilde{\mathbf{A}}_{\mathrm{v},\,i}\frac{\partial \mathbf{Q}}{\partial x_i} = \mathbf{0} \tag{11}$$

By introducing a Fourier mode $\mathbf{Q} = \mathbf{Q}_0 \exp\left[i(\mathbf{k}^T\mathbf{x} - \omega\tau)\right]$ into equation (11), the following equation for ω is obtained

$$\left(-i\omega\mathbf{I} + \frac{c_{k0}}{\Delta t}\boldsymbol{\Gamma}_{\mathrm{v}}^{-1}\frac{\partial \mathbf{U}}{\partial \mathbf{Q}} + ik_i\tilde{\mathbf{A}}_{\mathrm{v},\,i}\right)\mathbf{Q} = \mathbf{0} \tag{12}$$

where $\mathbf{I}$ is the identity matrix. Due to the finite number of mesh nodes, the wavelengths are limited by the grid spacing. To take this filtering into account, we can set $\|\mathbf{k}\| = \phi/h$, where h is a measure of the grid spacing, and $\phi \in [0, \pi]$. Let $\lambda = \omega/\|\mathbf{k}\|$ the wave speed and $u_k = \mathbf{u}^T\mathbf{k}/\|\mathbf{k}\|$. The system of equations $\hat{\mathbf{G}}\mathbf{Q} = \mathbf{0}$, where

$$\hat{\mathbf{G}} = -i\frac{c_{k0}}{\|\mathbf{k}\|\Delta t}\boldsymbol{\Gamma}_{\mathrm{v}}^{-1}\frac{\partial \mathbf{U}}{\partial \mathbf{Q}} + \frac{k_i}{\|\mathbf{k}\|}\tilde{\mathbf{A}}_{\mathrm{v},\,i} - \lambda\mathbf{I} \tag{13}$$

is obtained by dividing equation (12) by $i\|\mathbf{k}\|$. The equation $\hat{\mathbf{G}}\mathbf{Q} = \mathbf{0}$ will have a non-trivial solution if $\det(\hat{\mathbf{G}}) = 0$, which will occurs for certain values of λ, the eigenvalues of the following matrix

$$\mathbf{G} = -i\frac{c_{k0}}{\|\mathbf{k}\|\Delta t}\boldsymbol{\Gamma}_{\mathrm{v}}^{-1}\frac{\partial \mathbf{U}}{\partial \mathbf{Q}} + \frac{k_i}{\|\mathbf{k}\|}\tilde{\mathbf{A}}_{\mathrm{v},\,i} \tag{14}$$

Let the CFL numbers $CFL_u = u_k\Delta t/h$ and $CFL_c = c\Delta t/h$. Then, the eigenvalues of $\mathbf{G}$ could be computed analytically, giving

$$\begin{aligned} \lambda(\mathbf{G})_{1,\dots,n_{\mathrm{d}}} &= u_k(1 - ic_{k0}CFL_u^{-1}) \\ \lambda(\mathbf{G})_{n_{\mathrm{d}}+1,n_{\mathrm{d}}+2} &= \frac{u_k}{2}(1 - ic_{k0}CFL_u^{-1})T_{\pm} \end{aligned} \tag{15}$$

where

$$T_{\pm} = (1 + M_{\mathrm{r}}^2\chi) \pm \sqrt{(1 - M_{\mathrm{r}}^2\chi)^2 - 4M_{\mathrm{r}}^2\left[\frac{1}{(iM + c_{k0}CFL_c^{-1})^2} + 1 - \chi\right]} \tag{16}$$

and $\chi = \gamma - (\gamma - 1)\delta$.

When the ALE strategy is applied, the governing equations using the dual-time formulation are written as [20]

$$\mathbf{\Gamma}\frac{\partial \mathbf{U}}{\partial \tau} + \frac{\partial \mathbf{U}}{\partial t} + (\mathbf{A}_i - w_i\mathbf{I})\frac{\partial \mathbf{U}}{\partial x_i} = \frac{\partial}{\partial x_i}\left(\mathbf{K}_{ij}\frac{\partial \mathbf{U}}{\partial x_j}\right) + \mathbf{S} \tag{17}$$

where $\mathbf{w} = [w_1, \ldots, w_{n_d}]^T$ is the velocity of the reference system. Neglecting the diffusive and source terms in equation (17), we could perform the same procedure applied to equation (3) in order to compute analytically the eigenvalues for that system of equations. The eigenvalues of the resulting matrix

$$\mathbf{G}_{\mathrm{ALE}} = -i\frac{c_{k0}}{\|\mathbf{k}\|\Delta t}\mathbf{\Gamma}_{\mathrm{v}}^{-1}\frac{\partial \mathbf{U}}{\partial \mathbf{Q}} + \frac{k_i}{\|\mathbf{k}\|}\left(\tilde{\mathbf{A}}_{\mathrm{v},\,i} - w_i\mathbf{\Gamma}_{\mathrm{v}}^{-1}\frac{\partial \mathbf{U}}{\partial \mathbf{Q}}\right) \tag{18}$$

are the following

$$\begin{aligned} \lambda(\mathbf{G}_{\mathrm{ALE}})_{1,\ldots,n_{\mathrm{d}}} &= u_k(1 - ic_{k0}CFL_u^{-1}) - w_k \\ \lambda(\mathbf{G}_{\mathrm{ALE}})_{n_{\mathrm{d}}+1,n_{\mathrm{d}}+2} &= \frac{1}{2}[u_k(1 - ic_{k0}CFL_u^{-1}) - w_k]T_{\pm}^{\mathrm{ALE}} \end{aligned} \tag{19}$$

where

$$T_{\pm}^{\mathrm{ALE}} = (1 + M_{\mathrm{r}}^2\chi) \pm \sqrt{(1 - M_{\mathrm{r}}^2\chi)^2 - 4M_{\mathrm{r}}^2\left[\frac{1}{(i\bar{M} + c_{k0}CFL_c^{-1})^2} + 1 - \chi\right]} \tag{20}$$

$\bar{M} = (u_k - w_k)/c$, and $w_k = \mathbf{w}^T\mathbf{k}/\|\mathbf{k}\|$.

2.1. Preconditioning strategies

We will analyze different choices for the definition of the reference Mach number introduced in the expression of the preconditioning matrix (7). The analysis is performed using the ratio of maximum to minimum eigenvalues (ER) in modulus, computed as

$$ER = \frac{\max(|\lambda_i|)}{\min(|\lambda_i|)} \tag{21}$$

The ER relationship coincides with the condition number when the system is symmetrical and, in the case of a non-symmetrical system, gives a measure of the disparity in the wave-speeds.

The following three definitions of M_{r} are compared:

- Steady Preconditioning (SP): this case corresponds to the original proposal by Choi and Merkle [3], where

$$M_{\mathrm{r}}^{\mathrm{SP}} = \min(1, \max(M, M_\epsilon)) \tag{22}$$

  M_ϵ being a cut-off of the Mach number in the vicinity of stagnation points defined by the user.
- Unsteady Preconditioning (UP): in this case the reference Mach number is defined as suggested by Vigneron *et al.* [5]

$$M_{\mathrm{r}}^{\mathrm{UP}} = \min(1, \max(\sqrt{M^2 + CFL_c^{-2}}, M_\epsilon)) \tag{23}$$

- Non-preconditioning (NP): the unpreconditioned system could be recovered taking, when $\delta = 1$, $M_{\mathrm{r}}^{\mathrm{NP}} = 1$.

It is easy to see that $M_{\mathrm{r}}^{\mathrm{UP}} \to M_{\mathrm{r}}^{\mathrm{SP}}$ when $CFL_c \to \infty$ and, conversely, $M_{\mathrm{r}}^{\mathrm{UP}} \to M_{\mathrm{r}}^{\mathrm{NP}}$ when $CFL_c \to 0$. Hence, the UP is equivalent to the SP technique in the limit of large CFL_c numbers and to the unpreconditioned strategy for small CFL_c.

Figure 1 shows the ER ratio as a function of the CFL_c number for the inviscid case, *i.e.* using the eigenvalues given by equation (15), on which we take $c_{k0} = 1$, $\delta = 1$ ($\chi = 1$), $M_\epsilon = 1 \times 10^{-6}$ and $M = 1 \times 10^{-3}$.

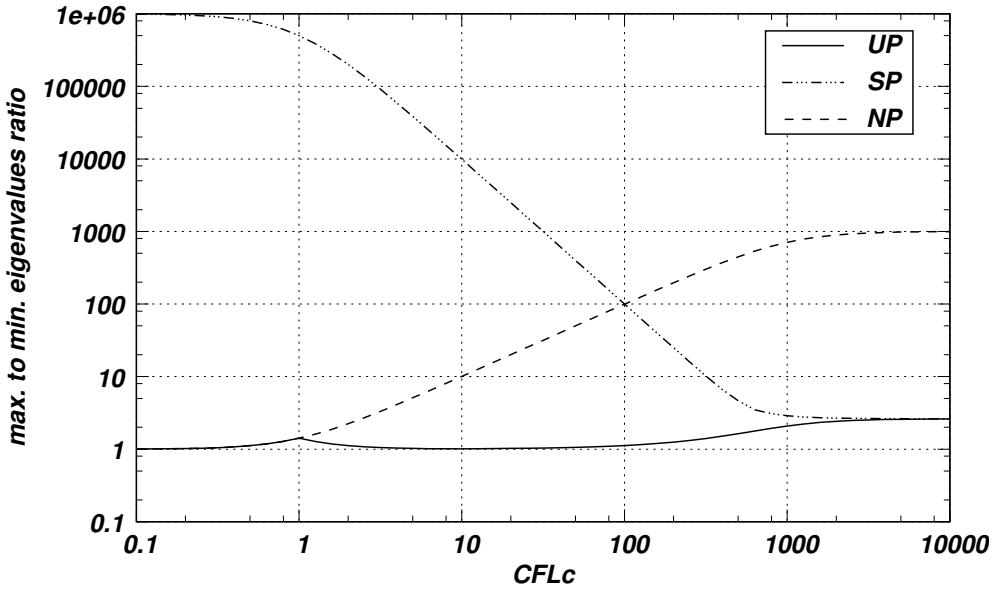

Figure 1. Maximum to minimum eigenvalues ratio as a function of CFL_c number with $M = 1 \times 10^{-3}$ and $M_\epsilon = 1 \times 10^{-6}$ for the inviscid case.

As could be observed in that figure, the unpreconditioned scheme is well suited for solving compressible flows if the CFL_c number is small enough. However, if the Mach number is too low, the system turns to be ill-conditioned as the CFL_c increases. On the other hand, the steady preconditioning leads to a small eigenvalues ratio for large CFL_c but this ratio increases when CFL_c tends to very small values. When the unsteady preconditioning is applied, the maximum to minimum eigenvalues ratio is $\mathcal{O}(1)$ for all CFL_c numbers.

For viscous flows is not longer easy to compute the eigenvalues of the preconditioned system (3). For this reason, many authors use approximations that depend on the Reynolds number [19, 5]. In this work, since the original definition of the preconditioning matrix includes some control of the time step in the viscous regions via the β parameter, we do not need to apply such approximations if $M_{\mathrm{r}}^{\mathrm{UP}}$ is used. We show this fact comparing the ER ratio as a function of the CFL_c and Re numbers for the three choices of the reference Mach number cited above. Since we do not have an analytical expression for the eigenvalues of the preconditioned system in the viscous case, the eigenvalues are computed numerically. The system (6) is Fourier

transformed keeping the viscous terms. The resulting matrix

$$\mathbf{G}_{\text{visc}} = -i\frac{c_{k0}}{\|\mathbf{k}\|\Delta t}\boldsymbol{\Gamma}_{\text{v}}^{-1}\frac{\partial \mathbf{U}}{\partial \mathbf{Q}} + \frac{k_i}{\|\mathbf{k}\|}\tilde{\mathbf{A}}_{\text{v},\,i} - i\frac{k_i k_j}{\|\mathbf{k}\|}\tilde{\mathbf{K}}_{\text{v},\,ij} \tag{24}$$

is then expressed in dimensionless form and, for given values of the dimensionless numbers, their eigenvalues are computed numerically using a calculus software (`Octave` [21]). Figure 2 shows the eigenvalues ratio as a function of CFL_c for several Reynolds numbers, where $c_{k0} = 1$, $\delta = 1$, $M_\epsilon = 1 \times 10^{-6}$ and $M = 1 \times 10^{-3}$. For Reynolds numbers above 10, the curves are very similar to those corresponding to the inviscid case. When the Reynolds number decreases below 0.1 the three curves tend to overlap, exhibiting the same behavior as function of the CFL_c number. In the range of Reynolds numbers between 0.1 and 10, the ER ratio behaves like in the inviscid case, *i.e.*, using M_{r}^{NP} as reference Mach number this ratio increases when the CFL_c increases and using M_{r}^{SP}, the ER ratio increases when the CFL_c decreases. In the same interval of variation of Reynolds and CFL_c numbers, the use of M_{r}^{UP} allows to keep the eigenvalues ratio $\mathcal{O}(1)$, as shown in figure 2.

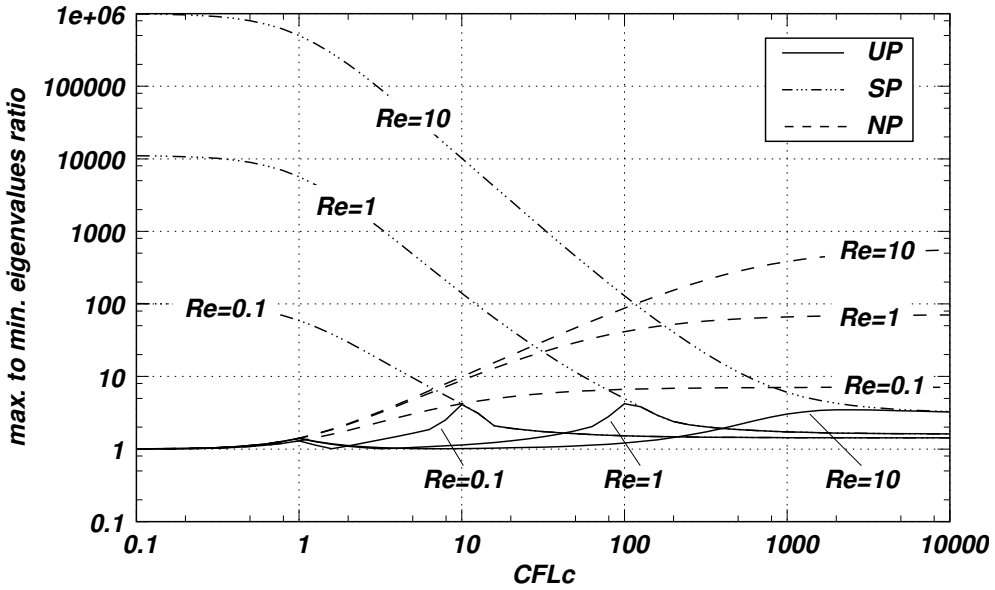

Figure 2. Maximum to minimum eigenvalues ratio as a function of CFL_c number for several Reynolds numbers, with $M = 1 \times 10^{-3}$.

3. NUMERICAL IMPLEMENTATION

3.1. Variational formulation

In this section, the variational formulation of the preconditioned Navier-Stokes equations for compressible flows is presented. The Finite Element Method (FEM) stabilized by means of the Streamline Upwind/Petrov-Galerkin (SUPG) strategy is used. Consider a finite element

discretization of the domain Ω into $n_{\rm el}$ sub-domains Ω^e, $e = 1, 2, \ldots, n_{\rm el}$. Based on this discretization, the finite element function spaces for the trial functions and for the weighting functions, $\mathscr{S}^h$ and $\mathscr{V}^h$ respectively, can be defined (see equation (26)). As was showed above, when the ALE technique is used only the advective jacobians are modified in the system of equations. Therefore, in order to simplify the notation, $\mathbf{w}$ velocity is considered null. The variational formulation of the problem is written as follows:

Find $\mathbf{U}^h \in \mathscr{S}^h$ such that $\forall\, \mathbf{W}^h \in \mathscr{V}^h$

$$\begin{aligned}
&\int_\Omega \mathbf{W}^h \left(\boldsymbol{\Gamma}^h \frac{\partial \mathbf{U}^h}{\partial \tau} + \frac{\partial \mathbf{U}^h}{\partial t} + \mathbf{A}_i^h \frac{\partial \mathbf{U}^h}{\partial x_i} \right) d\Omega + \int_\Omega \frac{\partial \mathbf{W}^h}{\partial x_i} \mathbf{K}_{ij}^h \frac{\partial \mathbf{U}^h}{\partial x_j} d\Omega \\
&+ \sum_{e=1}^{numel} \int_{\Omega^e} \boldsymbol{\tau}^T (\mathbf{A}_k^h)^T \frac{\partial \mathbf{W}^h}{\partial x_k} \left[\boldsymbol{\Gamma}^h \frac{\partial \mathbf{U}^h}{\partial \tau} + \frac{\partial \mathbf{U}^h}{\partial t} + \mathbf{A}_i^h \frac{\partial \mathbf{U}^h}{\partial x_i} - \frac{\partial}{\partial x_i} \left(\mathbf{K}_{ij}^h \frac{\partial \mathbf{U}^h}{\partial x_j} \right) - \mathbf{S} \right] d\Omega^e \\
&= \int_\Omega \mathbf{W}^h \mathbf{S} d\Omega + \int_{\Gamma^h} \mathbf{W}^h \mathbf{f} d\Gamma
\end{aligned} \tag{25}$$

where

$$\begin{aligned}
\mathscr{S}^h &= \{ \mathbf{U}^h | \mathbf{U}^h \in [\mathbf{H}^{1h}(\Omega)]^{n_{\rm dof}},\, \mathbf{U}^h|_{\Omega^e} \in [P^1(\Omega^e)]^{n_{\rm dof}},\, \mathbf{U}^h = \mathbf{g} \quad \text{on} \quad \Gamma^g \} \\
\mathscr{V}^h &= \{ \mathbf{W}^h | \mathbf{W}^h \in [\mathbf{H}^{1h}(\Omega)]^{n_{\rm dof}},\, \mathbf{W}^h|_{\Omega^e} \in [P^1(\Omega^e)]^{n_{\rm dof}},\, \mathbf{W}^h = \mathbf{0} \quad \text{on} \quad \Gamma^g \}
\end{aligned} \tag{26}$$

$\mathbf{H}^{1h}(\Omega)$ being the finite dimensional Sobolev functional space over Ω, with $\mathbf{f}$ and $\mathbf{g}$ representing the natural and Dirichlet boundary conditions vectors, respectively. Γ^g and Γ^h are the portions of the boundary with Dirichlet and Neumann conditions, respectively. $n_{\rm dof}$ stands for the number of degrees of freedom.

The derivative with respect to τ is discretized using the backward Euler difference scheme

$$\frac{\partial \mathbf{U}}{\partial \tau} \approx \frac{\mathbf{U}^{n+1,m+1} - \mathbf{U}^{n+1,m}}{\Delta \tau} \tag{27}$$

Notice the indeces used to indicate each time level: $n+1$ is the current physical time step and $m+1$ is the current pseudo-time step. In addition, an implicit formulation is proposed in both t and τ.

The definition of the matrix of intrinsic time scale $\boldsymbol{\tau}$ is very important in order to stabilize the numerical scheme correctly. In this work, we propose to apply the SUPG strategy, *i.e.* to stabilize the numerical scheme considering only the advective part of the system. The numerical diffusivity introduced by the SUPG method in the inviscid case is [22]

$$\tilde{\mathbf{K}}_{\rm v}^{\rm num} = \tilde{\mathbf{A}}_{\rm v} \tilde{\boldsymbol{\tau}}_{\rm v} \tilde{\mathbf{A}}_{\rm v} \tag{28}$$

where $\tilde{\boldsymbol{\tau}}_{\rm v}$ is the matrix of intrinsic time scale in the viscous variables basis. In the conservative variables basis this matrix is expressed as

$$\boldsymbol{\tau} = \frac{\partial \mathbf{U}}{\partial \mathbf{Q}} \tilde{\boldsymbol{\tau}}_{\rm v} \frac{\partial \mathbf{Q}}{\partial \mathbf{U}} \boldsymbol{\Gamma}^{-1} = \frac{\partial \mathbf{U}}{\partial \mathbf{Q}} \tilde{\boldsymbol{\tau}}_{\rm v} \boldsymbol{\Gamma}_{\rm v}^{-1} \tag{29}$$

For the computation of $\tilde{\boldsymbol{\tau}}_{\rm v}$ we propose to use an extension of the proposal by Le Beau *et al.* [23] to the preconditioned system considered in this work. This extension is written as follows

$$\tilde{\boldsymbol{\tau}}_{\rm v} = \frac{h/2}{\frac{1}{2}[\|\mathbf{u}\|(1 + \beta M_{\rm r}^2 \chi / c^2) + c']} \mathbf{I} \tag{30}$$

where $c' = \sqrt{\|\mathbf{u}\|^2 \left(1 + \frac{\beta M_\mathrm{r}^2 \chi}{c^2}\right)^2 + 4\beta M_\mathrm{r}^2 \left(1 - \frac{\|\mathbf{u}\|^2}{c^2}\right)}$ is the pseudo-acoustic speed. The denominator in the expression of the stabilization parameter is the maximum eigenvalue of the preconditioned advective jacobian, whose calculation can be found in [3] or [17]. The definition given by equation (30) is corrected in order to account for viscous effects (see, for instance, the work by Aliabadi *et al.* [24]).

The proposal given by equation (30) for the computation of $\tilde{\boldsymbol{\tau}}_\mathrm{v}$ differs from that used in [17, 16]. In these works, a stabilized FEM scheme is presented for the resolution of steady compressible flows for all Mach and Reynolds numbers, which utilizes the same preconditioning matrix applied here with M_r^SP as reference Mach number.

Remark 1. In the inviscid case (*i.e.* $\mu = 0$ and, thus, $\beta = c^2$), if the reference Mach number is adopted as M_r^NP, the pseudo-acoustic speed tends to $2c$ when $M \to 0$ and the expression for $\tilde{\boldsymbol{\tau}}_\mathrm{v}$ in (30) approaches to the corresponding expression of the unpreconditioned system $((h/2)/(\|\mathbf{u}\| + c))$. The same limit is reached when $M \to 1$, although in this case the three reference Mach numbers tends to 1.

Remark 2. Considering the unpreconditioned system ($M_\mathrm{r} = 1$) in the inviscid case, for the wave with a propagation speed of order $\|\mathbf{u}\|$ the numerical diffusion introduced by the stabilization strategy given by equation (30) is proportional to

$$\frac{h\|\mathbf{u}\|^2}{2(\|\mathbf{u}\| + c)} = \frac{h\|\mathbf{u}\|M}{2(1 + M)}$$

Thus, at the low Mach number limit, there are sub-stabilized modes due to the disparity in the wave-speeds. This sub-stabilization could leads to spurious numerical oscillations in the solution.

3.2. Dynamic boundary conditions

In this section we present briefly the treatment of the dynamic boundary conditions. We refer as dynamic boundary conditions to those boundary conditions that depend on the fluid state and/or the mesh state in the case of a problem with moving boundaries domain. In particular, we consider here the absorbing boundary conditions and a mixed absorbing/wall boundary condition.

As occurs with the stabilization term of the FEM formulation, the absorbing boundary conditions must be properly computed for the preconditioned system of equations. The idea here is to follow the proposal by Storti *et al.* [25] but applied to equation (6) expressed in the viscous variables basis. In multidimensional problems a simplified 1D analysis in the normal direction to the boundary is done by considering the projection of the advective jacobians onto this direction, as follows

$$\tilde{\mathbf{A}}_{\mathrm{v},\,n} = \tilde{\mathbf{A}}_{\mathrm{v},\,i} n_i \tag{31}$$

where n_i, $i = 1, \ldots, n_\mathrm{d}$ are the components of the unit vector normal to the local boundary. After diagonalization of the projected jacobian

$$\tilde{\mathbf{A}}_{\mathrm{v},\,n} = \tilde{\mathbf{M}}_\mathrm{v} \tilde{\boldsymbol{\Lambda}}_{\mathrm{v},\,n} \tilde{\mathbf{M}}_\mathrm{v}^{-1} \tag{32}$$

with $\tilde{\mathbf{\Lambda}}_{\mathrm{v},n} = \mathrm{diag}[\lambda(\tilde{\mathbf{A}}_{\mathrm{v},n})]$, the *projection matrices onto the right/left-going characteristics modes* in the diagonal basis are obtained

$$\begin{aligned} \left(\mathbf{\Pi}_V^-\right)_{ij} &= \begin{cases} 1 & \text{if } i=j \text{ and } \lambda_i(\tilde{\mathbf{A}}_{\mathrm{v},n}) < 0 \\ 0 & \text{otherwise} \end{cases} \\ \mathbf{\Pi}_V^- + \mathbf{\Pi}_V^+ &= \mathbf{I} \end{aligned} \tag{33}$$

The projection matrices in the viscous variables basis are computed changing the basis $\mathbf{\Pi}_Q^{\pm} = \tilde{\mathbf{M}}_{\mathrm{v}} \mathbf{\Pi}_V^{\pm} \tilde{\mathbf{M}}_{\mathrm{v}}^{-1}$. Finally, coming back to the $\mathbf{U}$ basis, the projection matrices are written as

$$\mathbf{\Pi}_U^{\pm} = \frac{\partial \mathbf{U}}{\partial \mathbf{Q}} \mathbf{\Pi}_Q^{\pm} \frac{\partial \mathbf{Q}}{\partial \mathbf{U}} \tag{34}$$

In this work, the absorbing boundary conditions are applied using Lagrange multipliers. Therefore, for a node i on the boundary, the system of equations to be solved is

$$\begin{aligned} &\mathbf{\Pi}_U^-(\mathbf{U}_{\mathrm{ref}})(\mathbf{U}_i - \mathbf{U}_{\mathrm{ref}}) + \mathbf{\Pi}_U^+(\mathbf{U}_{\mathrm{ref}})\mathbf{U}_{\mathrm{lm}} = \mathbf{0} \\ &\mathbf{R}_i(\mathbf{U}) + \mathbf{\Gamma}\mathbf{\Pi}_U^-(\mathbf{U}_{\mathrm{ref}})\mathbf{U}_{\mathrm{lm}} = \mathbf{0} \end{aligned} \tag{35}$$

where $\mathbf{U}_{\mathrm{ref}}$ is a reference state, $\mathbf{U}_{\mathrm{lm}}$ is the Lagrange multiplier, and $\mathbf{R}_i(\mathbf{U})$ is the FEM residue for the node i. The reference state must be specified by the user. If the external conditions are unknown, Storti *et al.* [25] propose to take $\mathbf{U}_{\mathrm{ref}}$ as the state of the fluid in the previous time step. They named this strategy ULSAR (Use Last State As Reference) and show that Riemann invariants are preserved in the limit $\Delta t \to 0$ and $h \to 0$, if such invariants exist.

The other kind of dynamic boundary condition that we consider is a mixed absorbing/wall condition. This type of condition could be useful in problems where the flow domain has moving boundaries. For instance, we use this mixed boundary condition for the computational simulation of internal combustion engines that utilize ports for the gas-exchange process, such as two-stroke and rotative (Wankel [26], MRCVC [27], etc.) engines. Generally, the ports are placed on fixed walls of the engine (the cylinder or the housing) and, thus, have a relative motion with respect to the flow domain.

Let consider a boundary node i that, due to the nodal displacement produced by the mesh deformation, could change their position between a solid wall and an inlet/outlet. In this case, the kind of boundary condition applied on node i must be changed appropriately in order to account for the relative node position in the boundary. The strategy used here consists in switching from an absorbing boundary condition (equation (35)) when the node is placed on the inlet/outlet region to a wall boundary condition when the node moves to the solid wall. In such a case, the wall boundary condition is applied via constraints using Lagrange multipliers in order to keep constant the total number of degrees of freedom. For instance, in a 3D problem using a no-slip boundary condition on a still solid wall, the system of equations for the node i when it is located on the solid wall is written as

$$\begin{aligned} &\mathbf{M}\mathbf{U}_i + (\mathbf{I} - \mathbf{M})\mathbf{U}_{\mathrm{lm}} = \mathbf{0} \\ &\mathbf{R}_i(\mathbf{U}) + \mathbf{M}\mathbf{U}_{\mathrm{lm}} = \mathbf{0} \end{aligned} \tag{36}$$

where $\mathbf{M} = \mathrm{diag}[0,1,1,1,0]$.

4. NUMERICAL RESULTS

The unsteady local preconditioning strategy presented was applied to several problems. Among the solved problems, there are steady and unsteady incompressible flows with moving domains. The purpose of these problems was to compare the preconditioned-system solution and the solution obtained by using a standard incompressible Navier-Stokes code. Furthermore, a test inherently compressible, which is the simulation of the in-cylinder flow in an opposed-piston internal combustion engine under cold conditions, is presented.

The pseudo-time step is increased during the pseudo-transient following the rule

$$\Delta\tau^{m+1} = \Delta\tau^{0}\frac{\|\mathbf{R}^{0}\|}{\|\mathbf{R}^{m}\|} \tag{37}$$

where $\mathbf{R}$ is the global residue and $\Delta\tau^0$ is an initial pseudo-time step defined by the user.

4.1. Flow in a lid driven cavity

This test served as a benchmark for the Navier-Stokes equations for incompressible flow for decades. The problem consists in a fluid into a square cavity with length side L and whose top wall moves with a uniform velocity U. Two Reynolds numbers ($Re = \rho UL/\mu$) cases 100 and 1000 are considered and a 60×60 quadrangles mesh is employed. A uniform grid is used for $Re = 100$, while a stretched grid is used for $Re = 1000$, with a ratio of 1:10 between elements near the wall and elements in the central region of the domain. The Mach number of the moving lid is 4.5×10^{-4}. No-slip boundary condition is applied on solid walls, which are assumed isothermic. Initially, the fluid is at rest and its pressure and temperature are constants, with values of 1×10^5 Pa and 300 K respectively. The test was solved with the unsteady preconditioning strategy and, in order to compare, solving the Navier-Stokes equations for incompressible flow (NSI). The incompressible Navier-Stokes equations are solved using FEM stabilized by means of the SUPG [28] and the Pressure-Stabilizing/Petrov-Galerkin (PSPG) [29] methods. Since this test tends to a steady state when $t \to \infty$, we use a large CFL_c number in the computation. Under this condition, the steady preconditioning and the unsteady preconditioning strategies are equivalent. However, we proposed to solve this case in order to test the stabilization coefficient introduced in equation (30).

Figures 3 and 4 show the magnitude of the velocity and the pressure perturbation, respectively. The pressure perturbation is computed as $p - \bar{p}$, with $\bar{p} = 1 \times 10^5$ Pa. Notice that the solution obtained is smooth and with no numerical oscillations.

In order to verify the accuracy of the UP method, the velocity profiles at vertical and horizontal centerlines of cavity ($x_1/L = 0.5$ and $x_2/L = 0.5$, respectively) are compared with a numerical solution of the incompressible Navier-Stokes equations by Ghia *et al.* [30]. The u_1 velocity is compared at the vertical centerline of the cavity, and the u_2 velocity is compared at the horizontal centerline of the cavity. Figures 5 and 6 show the results, where good agreement can be observed.

4.2. Flow in a channel with a moving indentation

This test case consists in a flow through a 2D channel with a moving indentation, which has been studied experimentally by Pedley and Stephanoff [31], and numerically by Ralph and Pedley [32] and by Demirdžić and Perić [33].

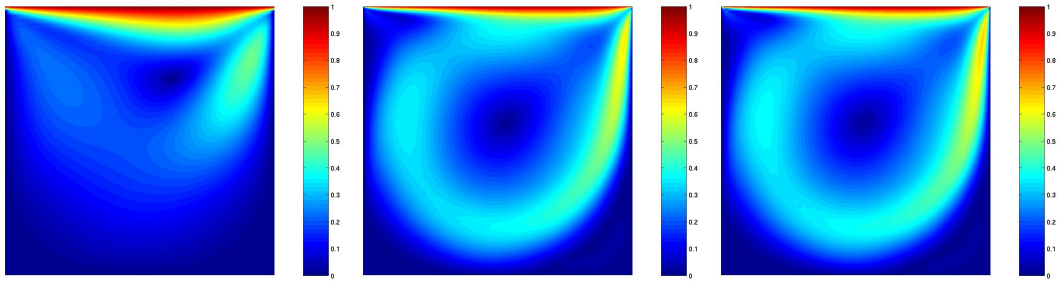

(a) $Re = 100$ - UP (b) $Re = 1000$ - UP (c) $Re = 1000$ - NSI

Figure 3. Non-dimensional magnitude of the velocity field ($\|\mathbf{u}\|/U$) for the flow in a lid driven cavity.

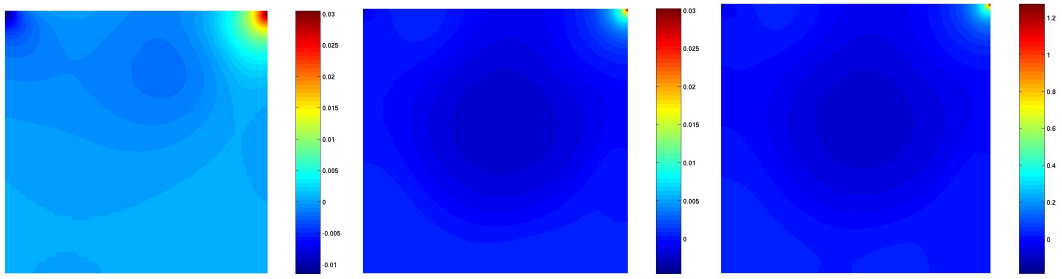

(a) $Re = 100$ - UP (b) $Re = 1000$ - UP (c) $Re = 1000$ - NSI

Figure 4. Pressure perturbation field ([Pa]) for the flow in a lid driven cavity.

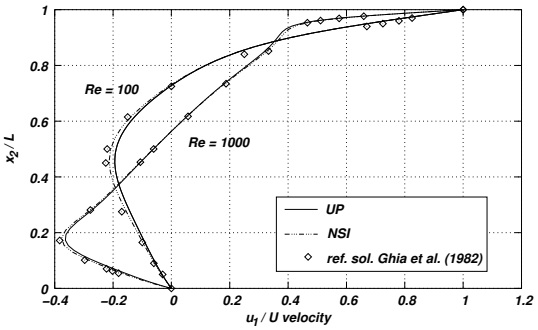

Figure 5. Comparison of u_1 velocity component at vertical centerline of the cavity with numerical solution by Ghia *et al.* [30].

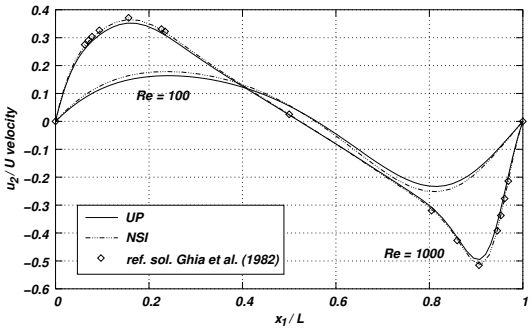

Figure 6. Comparison of u_2 velocity component at horizontal centerline of the cavity with numerical solution by Ghia *et al.* [30].

Figure 7 shows a scheme of the channel geometry. The shape of the indentation is taken from Pedley and Stephanoff [31], who specified the following analytic function which approximately

fit the real shape used in the experiment

$$x_2(x_1) = \begin{cases} h & \text{for } 0 \le x_1 < d_1 \\ 0.5h\{1 - \tanh[a(x_1 - d_2)]\} & \text{for } d_1 \le x_1 \le d_3 \\ 0 & \text{for } x_1 > d_3 \end{cases}$$

where $a = 4.14$, $d_1 = 4b$, $d_3 = 6.5b$, $d_2 = 0.5(d_1 + d_3)$, and

$$h = 0.5h_{\max}[1 - \cos(2\pi t^*)] \tag{38}$$

being $t^* = \dfrac{t - t_0}{\Upsilon}$. Here b is the channel height, Υ is the oscillation period and $h_{\max} = 0.38b$

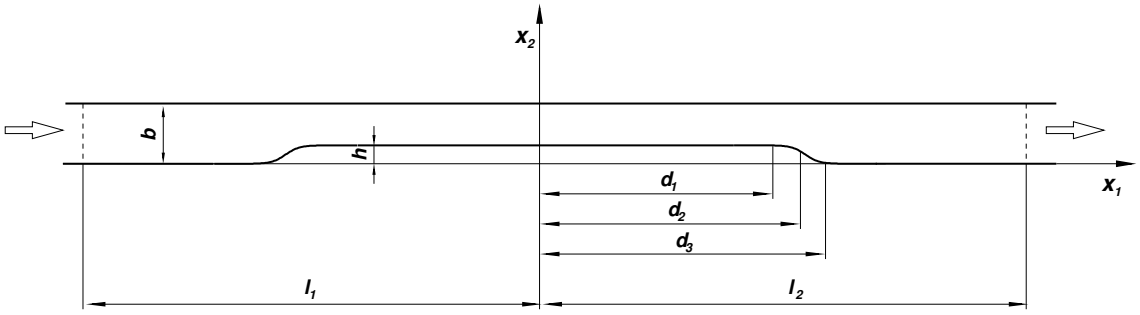

Figure 7. Geometry of the channel (not to scale): $b = 1$ cm, $l_1 = 9.85$ cm, $l_2 = 18.0$ cm.

specifies the maximum blockage of the channel cross-section at $t^* = 0.5$. The geometry is symmetric around $x_1 = 0$. The Strouhal number based on the channel height, bulk velocity $U = (2/3)u_{\max}$ and oscillation period,

$$St = \frac{b}{U\Upsilon}, \tag{39}$$

is 0.037. The Reynolds number based on the same reference quantities is 507. At the initial time $t = t_0$ the flow is assumed to be fully developed (Poiseuille flow). The maximum velocity is $u_{\max} = 1.5$ m/s. The velocity profile at the inlet cross-section is taken to remain constant throughout the cycle. Also a constant density is imposed at the inlet cross-section ($\rho_{\text{inlet}} = 1.1614$ kg/m^3). At the other channel end, dynamic boundary conditions with the ULSAR strategy were imposed, as presented in section 3.2. Walls are assumed isothermic (300 K) and no slip boundary condition is imposed on them. Mesh dynamics was solved applying the method proposed by López *et al.* [34], which consists in minimizing the mesh element distortion. The mesh used has 12362 triangular elements and 6759 nodes. The (physical) time step adopted in the simulation was $\Delta t = \Upsilon/200$.

Figures 8, 9 and 10 show the density field, the magnitude of the flow velocity, and the pressure perturbation (with $\bar{p} = 1 \times 10^5$ Pa) at the times $t^* = 0.2$, 0.3, 0.4, 0.5, 0.6, 0.7, 0.8, 0.9 and 1 for the UP strategy.

Table I compares the solution obtained using the unsteady preconditioning strategy and two solutions of the Navier-Stokes equations for incompressible flow. The comparison is done taking the maximum velocity during the cycle and the time in which the three first vortices appear.

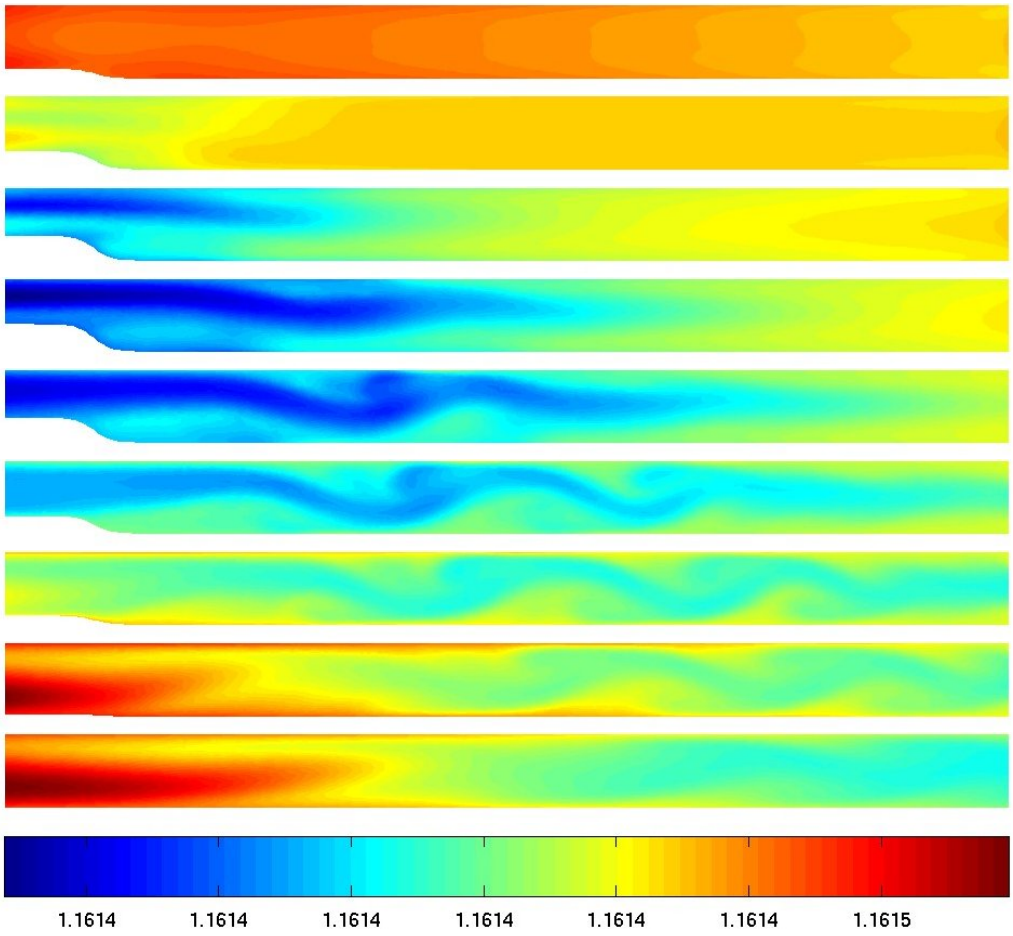

Figure 8. Density field ([kg/m^3]) for the flow in a channel with a moving indentation computed using the UP strategy. From top to bottom, times $t^* = 0.2$, 0.3, 0.4, 0.5, 0.6, 0.7, 0.8, 0.9 and 1.

	UP	López *et al.* [34]	Demirdžić and Perić [33]
Max. velocity [m/s]	2.916 at $t^* = 0.37$	2.931 at $t^* = 0.38$	2.645 at $t^* = 0.4$
1$^{\text{st}}$ vortex	$t^* = 0.22$	$t^* = 0.23$	$t^* = 0.2$-0.25
2$^{\text{nd}}$ vortex	$t^* = 0.345$	$t^* = 0.35$	$t^* = 0.35$-0.4
3$^{\text{rd}}$ vortex	$t^* = 0.425$	$t^* = 0.42$	$t^* = 0.45$

Table I. Comparison of results obtained using the UP strategy and two solutions of the incompressible Navier-Stokes equations for the channel with a moving indentation test.

Figure 11 shows the positions of the first three eddies center as a function of time. In that figure, the experimental data reported by Pedley and Stephanoff [31] and the numerical solutions of the UP technique and the Navier-Stokes equations for incompressible flow [34] are

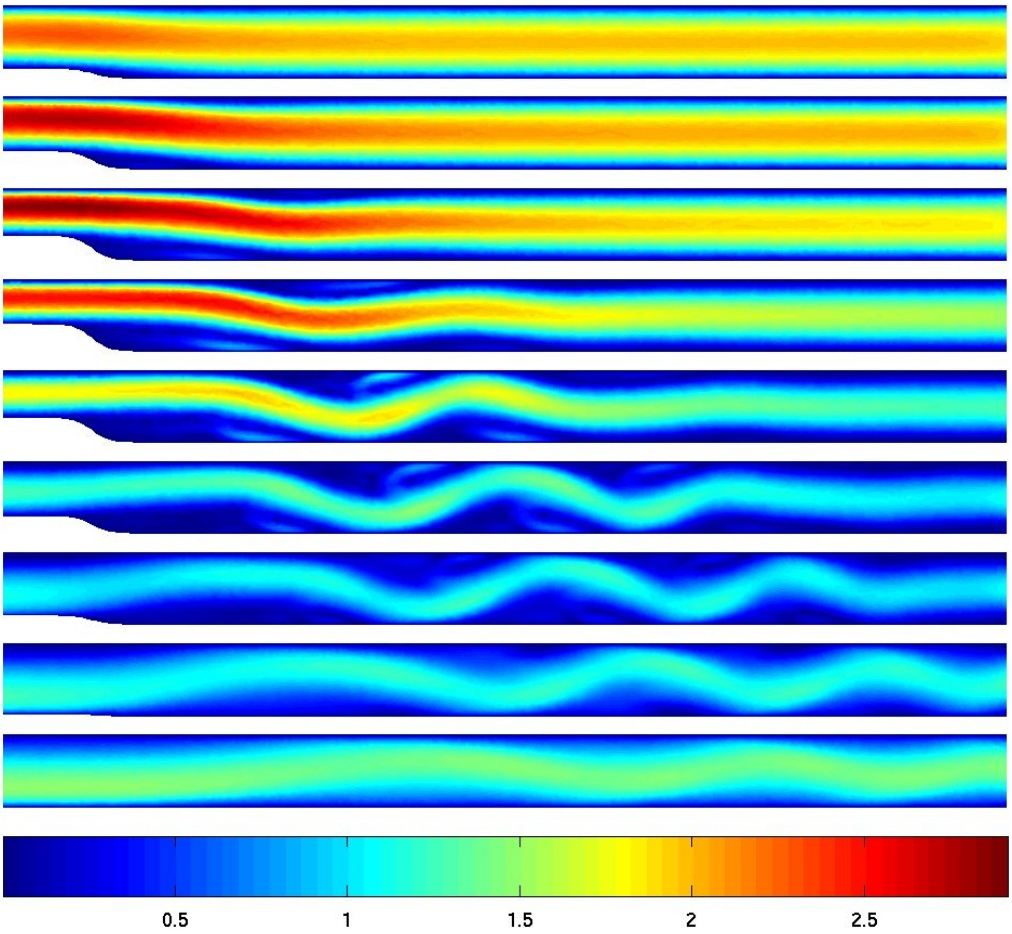

Figure 9. Magnitude of the flow velocity field ([m/s]) for the flow in a channel with a moving indentation computed using the UP strategy. From top to bottom, times $t^* = 0.2$, 0.3, 0.4, 0.5, 0.6, 0.7, 0.8, 0.9 and 1.

included. According to Pedley and Stephanoff [31], the abscissa was defined as

$$x_1^* = \frac{(x_1 - d_1)(10St)^{1/3}}{b} \tag{40}$$

This test may be useful to compare the solutions obtained by means the three choices of M_r in the preconditioning matrix. The solution correspondig to the unsteady preconditioning system is adopted as reference and is compared with the solutions of the other two strategies.

In first place we compare the UP and NP solutions. As expected, the unpreconditioned solution does not represent the behavior of the flow since it does not produce the different vortices experimentally observed. In addition, the pressure field presents numerical oscillations which could be observed in figure 12. In that figure, the isolines of the pressure perturbation fields (with $\bar{p} = 1 \times 10^5$) for $t^* = 0.5$ computed with the UP and NP strategies are shown.

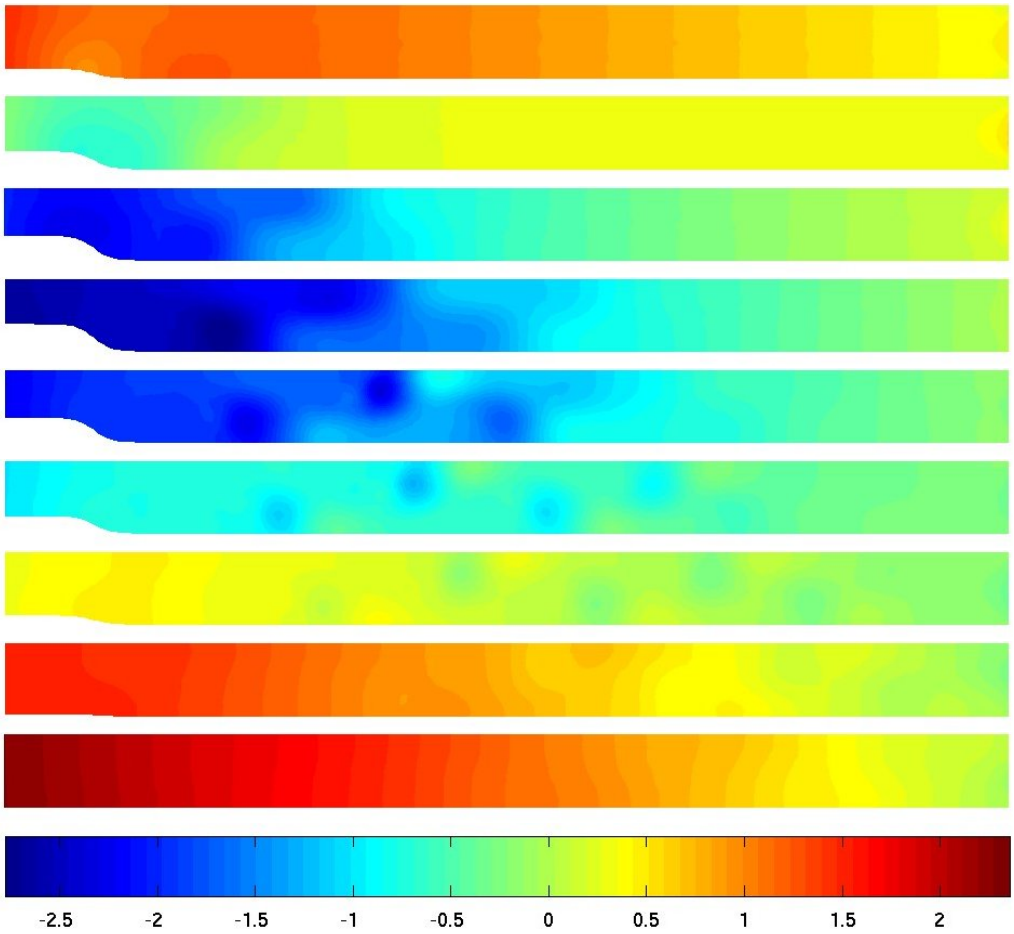

Figure 10. Pressure perturbation field ([Pa]) for the flow in a channel with a moving indentation computed using the UP strategy. From top to bottom, times $t^* = 0.2$, 0.3, 0.4, 0.5, 0.6, 0.7, 0.8, 0.9 and 1.

The top sub-figure corresponds to the unsteady preconditioning solution, while the middle sub-figure corresponds to the unpreconditioned system with the same parameters as presented above (same Δt, mesh, etc.). With the aim to avoid the numerical oscillations, we decreased the time step by a factor of 10. In the bottom sub-figure of figure 12 the isolines of the pressure perturbation field computed with the unpreconditioned system with $\Delta t = \Upsilon/2000$ are shown. As could be observed, this solution also presents numerical oscillations. We conclude that the spurious numerical oscillations are due to the sub-stabilization introduced by the way in which the matrix of intrinsic time scale is computed (see equation (30) and remark 2 at the end of section 3.1).

The difference between UP and SP methods is given by the CFL_c number only. Therefore, keeping the same mesh and the conditions of the fluid, the unique parameter of the simulation that distinguishes both techniques is the physical time step. Using the original set of parameters ($\Delta t = \Upsilon/200$) the CFL_c number is $\mathcal{O}(10^3)$. Then, as predicted by theory in figures 1 and 2,

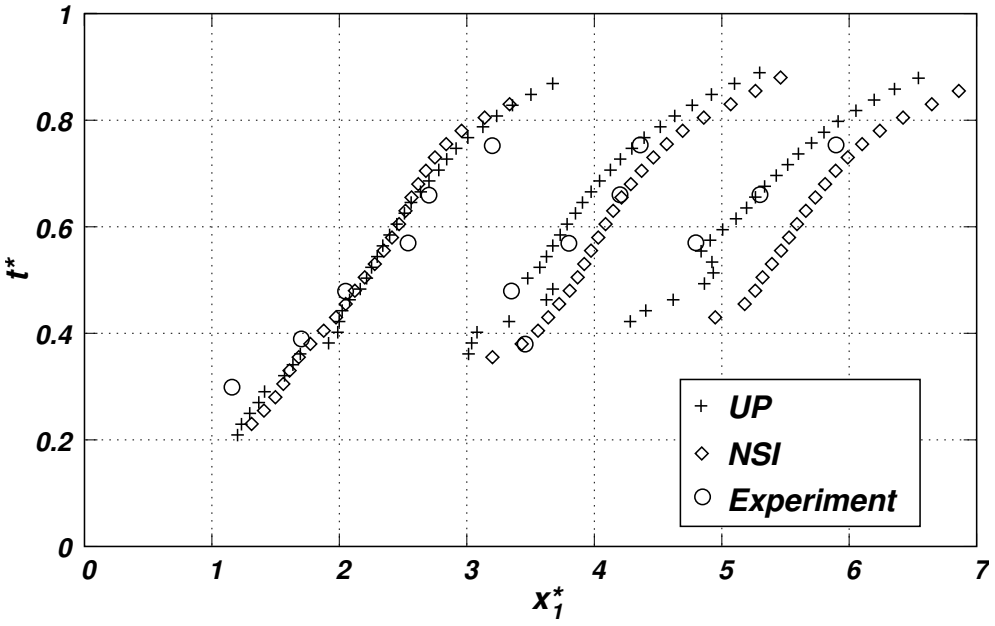

Figure 11. Comparison of predicted and experimentally observed positions of the first three vortices center.

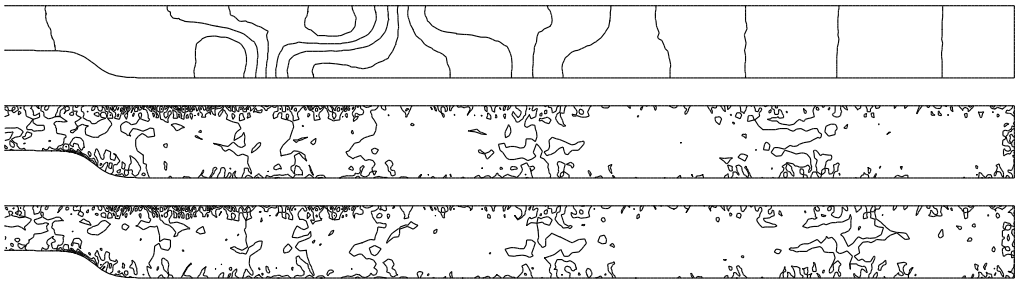

Figure 12. Isolines of the pressure perturbation field at $t^* = 0.5$ for the flow in a channel with a moving indentation computed with the UP (top, $\Delta t = \Upsilon/200$) and NP ($\Delta t = \Upsilon/200$, middle; $\Delta t = \Upsilon/2000$, bottom) strategies.

the unsteady and steady preconditioning strategies are almost equivalent and they give very similar solutions. However, if the time step is decreased the steady preconditioning method fails to give an acceptable solution and, according with our experiments, the execution of the code is interrupted by insurmountable errors. For instance, with a time step ten times smaller than the original one ($\Delta t = \Upsilon/2000$, for which CFL_c is $\mathcal{O}(10^2)$) the run breaks down before completing the first half of period. Figure 13 shows some contour lines of pressure perturbation and density fields at $t^* = 0.41$ (a few time steps before the interruption of the code execution) computed with the steady preconditioning strategy. With comparison purposes, the figure include the respective isolines of the state obtained by solving the problem with the UP technique. As could be observed, the solution of the SP strategy presents spurious oscillations that begin to

form in the vicinity of the vortices centers.

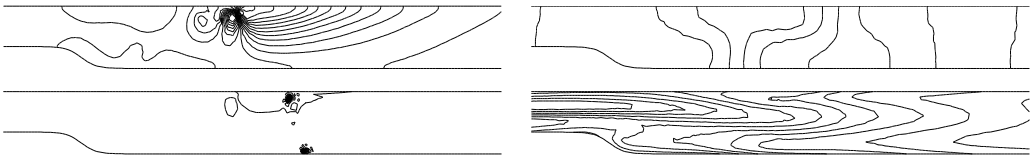

Figure 13. Isolines of the pressure perturbation (top) and density (bottom) fields at $t^* = 0.41$ for the flow in a channel with a moving indentation computed with the SP (left) and UP (right) strategies. Solutions computed with $\Delta t = \Upsilon/2000$.

Regarding the computational cost, we compare the cumulated computational time used to simulate the time interval corresponding to the cycle Υ with the UP and NP strategies. The results are presented in figure 14. The computational times are relative to the total elapsed time employed by the unsteady preconditioning strategy. Although this strategy is computationally more costly than the unpreconditiong technique (with the same set of parameters), when the time step is decreased by a factor of 10 the cumulated computational relative time increases 9 times approximately. For the unpreconditiong method the $CFL = (M+1)CFL_c$ number determines the appropriate time step for the simulation, while for the unsteady preconditioning strategy we could control the CFL_u and CFL_c numbers. Let Δt_{NP} and Δt_{UP} the time steps computed for the NP and UP strategies, respectively. In the low-Mach number limit $CFL \approx CFL_c$. Now, suppose we take the CFL number for the NP technique equal to the CFL_u for the UP strategy. Then $\Delta t_{\mathrm{NP}} = M\Delta t_{\mathrm{UP}}$, and for the unpreconditioning strategy the computational cost could be significantly high.

4.3. Opposed-piston engine

The last case presented is the resolution of the fluid flow inside the cylinder of an opposed-piston engine under cold conditions, *i.e.* without combustion. This test was selected in order to show the application of the unsteady preconditioning strategy to an inherently compressible case. The engine geometry was taken from the KIVA-3 [35] tutorial. The cylinder bore is 100 mm, the stroke of each piston is 85 mm, and the geometric compression ratio is 9.5:1. The cylinder has 8 exhaust ports evenly distributed in the circumferential direction and 12 intake ports uniformly separated also. Assuming the reference angle as the EDC (External Dead Center), the timing of the ports are the following

- Intake Port Opening (IPO) = 295.13°
- Intake Port Closing (IPC) = 64.87°
- Exhaust Port Opening (EPO) = 280.2°
- Exhaust Port Closing (EPC) = 79.8°

In order to simplify the problem, the flow domain is assumed to have axial symmetry around the cylinder axis. The domain is not axisymmetric since the intake and exhaust ports are not continuously distributed as a 'ring' around the cylinder. However, the proposed simplification is perfectly valid for the purpose of this paper. The simplified geometry is shown in figure 15 for pistons located at EDC.

The mesh was generated with the pistons at EDC (ports totally opened) and has 19K hexahedra and 38.6K nodes. The mean element size is $h = 1$ mm. Due to the simplicity of the

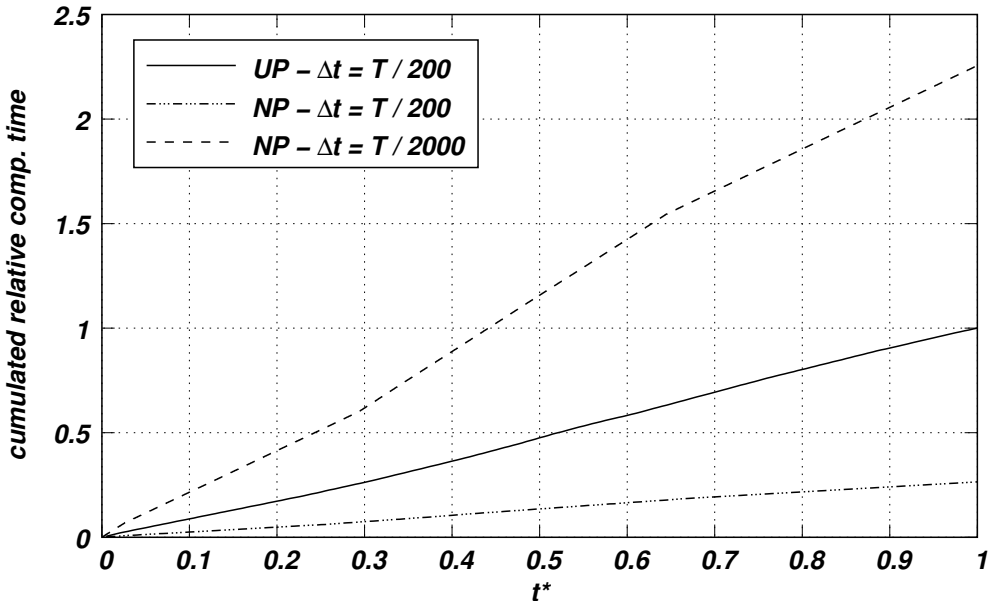

Figure 14. Comparison of the cumulated computational time employed for the simulation of the first cycle in the channel with a moving indentation problem. The computational time shown is relative to the elapsed time for the UP strategy.

geometry and the boundary movement, the mesh dynamics is solved using an algebraic law following a linear distribution with respect to the position of pistons at IDC (Internal Dead Center).

No-slip condition is imposed at solid walls. In addition, these walls are assumed insulated. Mixed absorbing/wall boundary conditions are used to model the ports, as explained in section 3.2. For absorbing boundary conditions, the reference state used for the intake port is $\mathbf{Q}^i_{\text{ref}} = [105\,\text{kPa}, \mathbf{0}\,\text{m/s}, 300\,\text{K}]^T$, and for the exhaust port is $\mathbf{Q}^e_{\text{ref}} = [95\,\text{kPa}, \mathbf{0}\,\text{m/s}, 500\,\text{K}]^T$. In this case, we model the turbulence applying the simplest LES (Large Eddy Simulation) Smagorinsky model [36, 37], which takes the Smagorinsky coefficient as constant. The engine speed is 3000 rpm. The time step used in the simulation was selected with the goal to keep CFL_u $\mathcal{O}(1)$ along the whole simulation, but bounded below by a minimum time step corresponding to 0.25 crank angle degrees (CAD) and bounded above by a maximum time step equivalent to 3 CAD. The stationary cyclic state is reached with approximately three cycles. The test was solved applying the UP strategy, since the Mach number could vary from very low values to values of order 0.5.

For some instants in the cycle, the density, pressure and Mach number fields into the chamber are depicted in the following figures, which correspond to the last cycle simulated. The position of the pistons in these moments is sketched in figure 16. The purpose is to show that the unsteady preconditioning strategy presented above produces smooth solutions (without numerical oscillations) when it is applied to computations of in-cylinder flows problems. Figures 17, 18 and 19 show the distribution of density, pressure and Mach number into the cylinder at 60 CAD (when the intake phase approaches the end), 130 CAD (the half of the

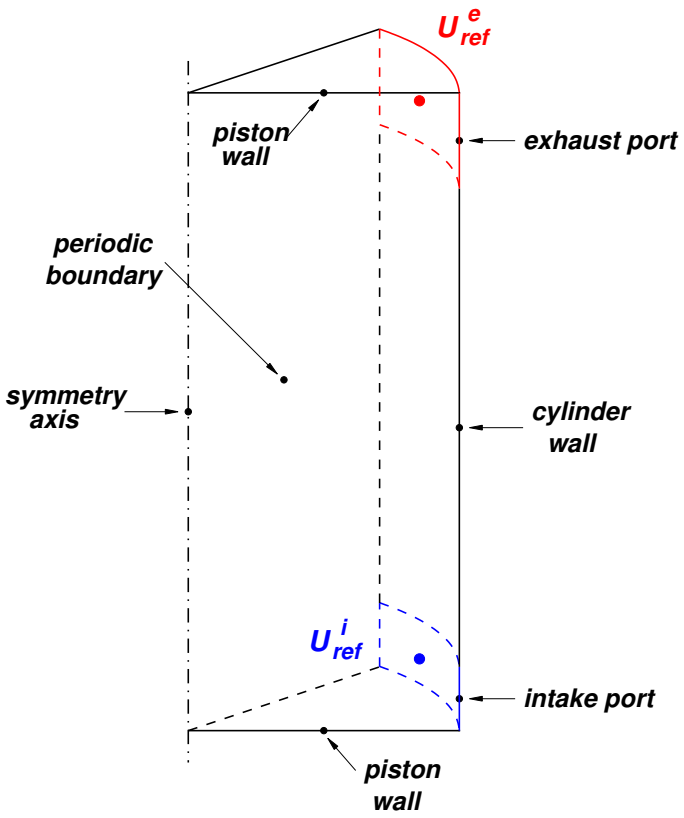

Figure 15. Geometry of the simplified axisymmetric model for the opposed-piston engine case (pistons at EDC).

compression stroke) and 321 CAD (pass half of the exhaust period), respectively.

5. CONCLUSIONS

The method of preconditioning of the equations was applied in conjunction with the dual-time-stepping strategy in order to solve transient flow problems at low Mach numbers in deformable domains. The application of a preconditioning matrix originally designed for steady compressible viscous flows was studied. Some definitions of one of the adjustable parameters of that matrix were analyzed using the eigenvalues of the system. A stabilized SUPG Finite Element method was formulated, in which was proposed to compute the stabilization parameter using the maximum eigenvalue of the preconditioned advective jacobians. The dynamic boundary conditions problem was also addressed, where dynamic absorbing conditions are applied on inlet/outlet boundaries and mixed absorbing/wall are used to model intake and exhaust ports in internal combustion engines. The resultant method was applied to incompressible flows and compared with solutions of the incompressible Navier-Stokes equations with very good results. Furthermore, the strategy was tested in an

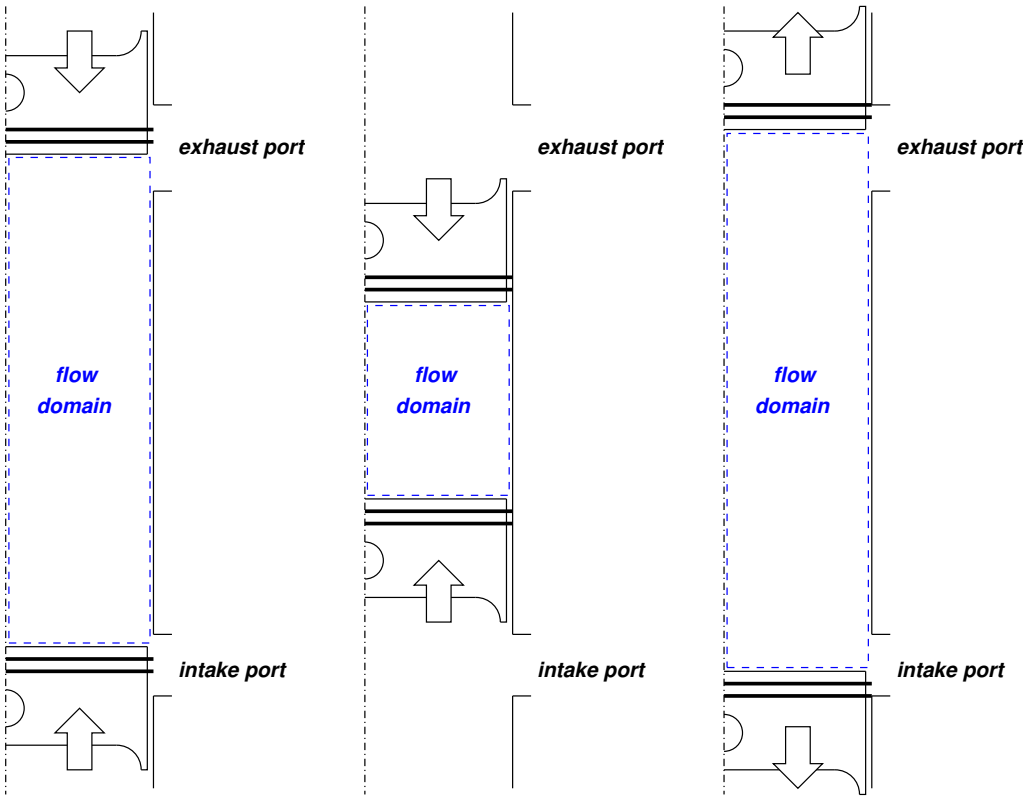

(a) 60 CAD (state shown in figure 17)

(b) 130 CAD (state shown in figure 18)

(c) 321 CAD (state shown in figure 19)

Figure 16. Sketchs of the pistons position for the instants during the cycle for which the state of the fluid is shown.

axisymmetric opposed-piston engine problem under cold conditions.

ACKNOWLEDGEMENTS

This work has received financial support from Consejo Nacional de Investigaciones Científicas y Técnicas (CONICET, Argentina, grants PIP 5271/05), Universidad Nacional del Litoral (UNL, Argentina, grant CAI+D 2005-10-64) and Agencia Nacional de Promoción Científica y Tecnológica (ANPCyT, Argentina, grants PICT 12-14573/2003, PME 209/2003). Authors made extensive use of freely distributed software as GNU/Linux OS, MPI, PETSc, GCC compilers, Octave, Perl, among many others.

REFERENCES

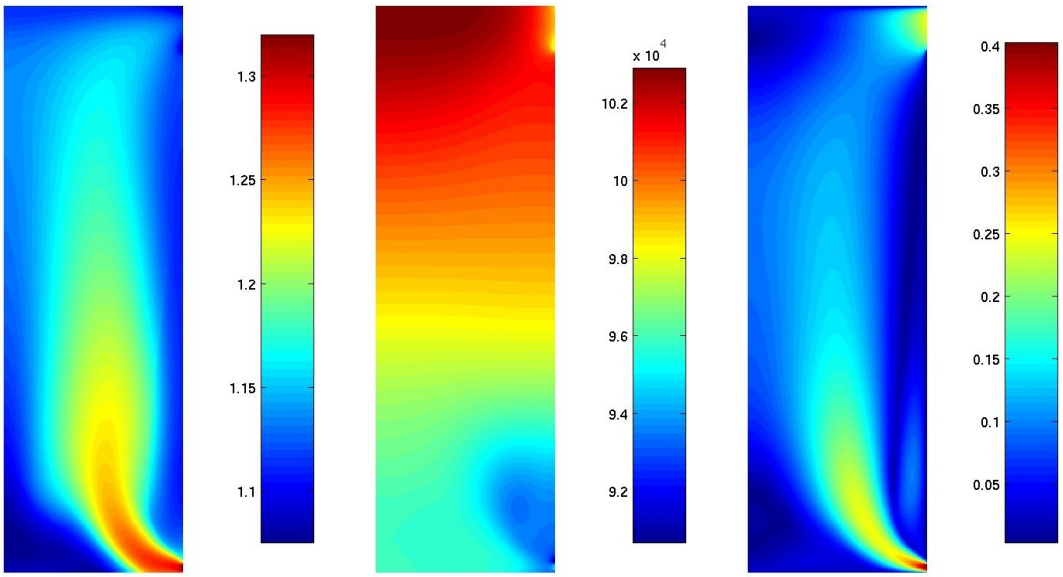

(a) Density [kg/m^3] (b) Pressure [Pa] (c) Mach number

Figure 17. State of the flow at the end of the intake phase (60 CAD) in the axisymmetric opposed-piston engine test computed with the UP strategy.

1. Turkel E. Preconditioned methods for solving the incompressible and low speed compressible equations. *Journal of Computational Physics* 1987; **72**(2):277–298.
2. Merkle CL, Choi YH. Computation of low-speed compressible flows with time-marching procedures. *International Journal for Numerical Methods in Engineering* 1988; **25**(2):293–311.
3. Choi YH, Merkle C. The application of preconditioning in viscous flows. *Journal of Computational Physics* 1993; **105**:207–223.
4. Xu X, Lee JS, Pletcher RH. A compressible finite volume formulation for large eddy simulation of turbulent pipe flows at low Mach number in Cartesian coordinates. *Journal of Computational Physics* 2005; **203**:22–48.
5. Vigneron D, Deliége G, Essers J-A. Low Mach number local preconditioning for unsteady viscous finite volumes simulations on 3D unstructured grids. *European Conference on Computational Fluid Dynamics* 2006.
6. Liu K, Pletcher R. A fractional step method for solving the compressible Navier-Stokes equations. *Journal of Computational Physics* 2007; **226**:1930–1951.
7. Harlow FH, Amsden AA. A numerical fluid dynamics calculation method for all flow speeds. *Journal of Computational Physics* 1971; **8**(2):197–213.
8. Issa RI, Gosman AD, Watkins AP. The computation of compressible and incompressible recirculating flows by a non-iterative implicit scheme. *Journal of Computational Physics* 1986; **62**(1):66–82.
9. Karki KC, Patankar SV. Pressure based calculation procedure for viscous flows at all speeds in arbitrary configurations. *AIAA Journal* 1989; **27**(9):1167–1174.
10. Mittal S, Tezduyar TE. A unified finite element formulation for compressible and incompressible flows using augmented conservation variables. *Computer Methods in Applied Mechanics and Engineering* 1998; **161**: 229–243.
11. Merkle CL, Choi YH. Computation of low-speed flow with heat addition. *AIAA Journal* 1987; **25**(6):831–838.
12. Merkle CL, Athavale M. Time-accurate unsteady incompressible flow algorithms based on artificial compressibility. *AIAA Paper* 87-1137, 1987.

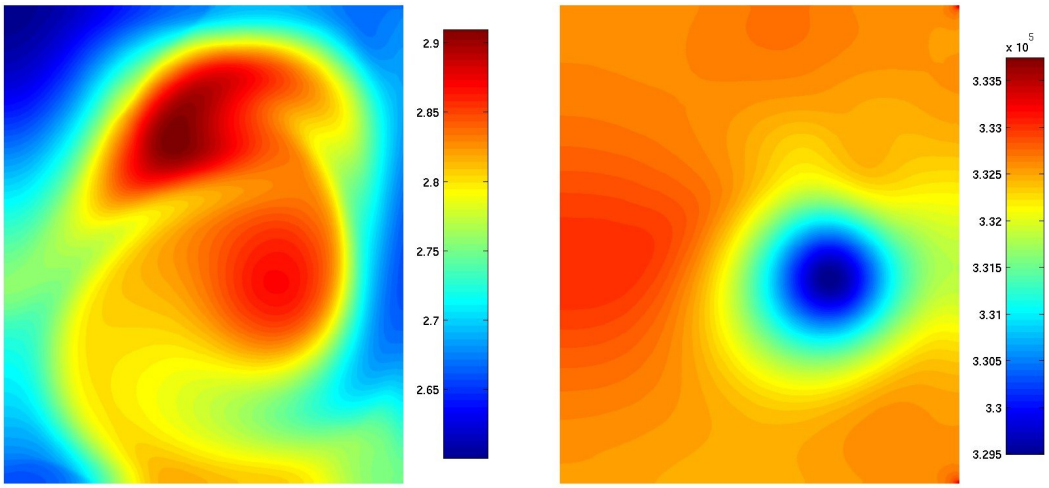

(a) Density [kg/m^3] (b) Pressure [Pa]

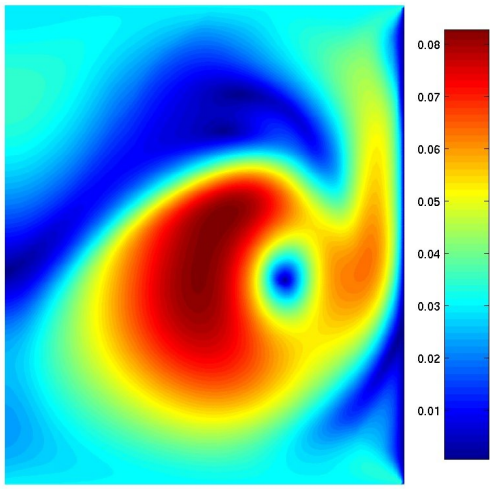

(c) Mach number

Figure 18. State of the flow at half of the compression stroke (130 CAD) in the axisymmetric opposed-piston engine test computed with the UP strategy.

13. Jameson A. Time dependent calculations using Multigrid with application to unsteady flows past airfoils and wings. *AIAA Paper* 91-1596, 1991.
14. Turkel E, Vasta V. Local preconditioners for steady and unsteady flow applications. *ESAIM: Mathematical Modelling and Numerical Analysis* 2005; **39**:515–535.
15. Turkel E, Radespiel R, Kroll N. Assessment of preconditioning methods for multidimensional aerodynamics. *Computers & Fluids* 1997; **26**(6):613–634.
16. Nigro N, Storti M, Idelsohn S. GMRES physics-based preconditioner for all Reynolds and Mach numbers: numerical examples. *International Journal for Numerical Methods in Engineering* 1997; **25**:1374–1371.

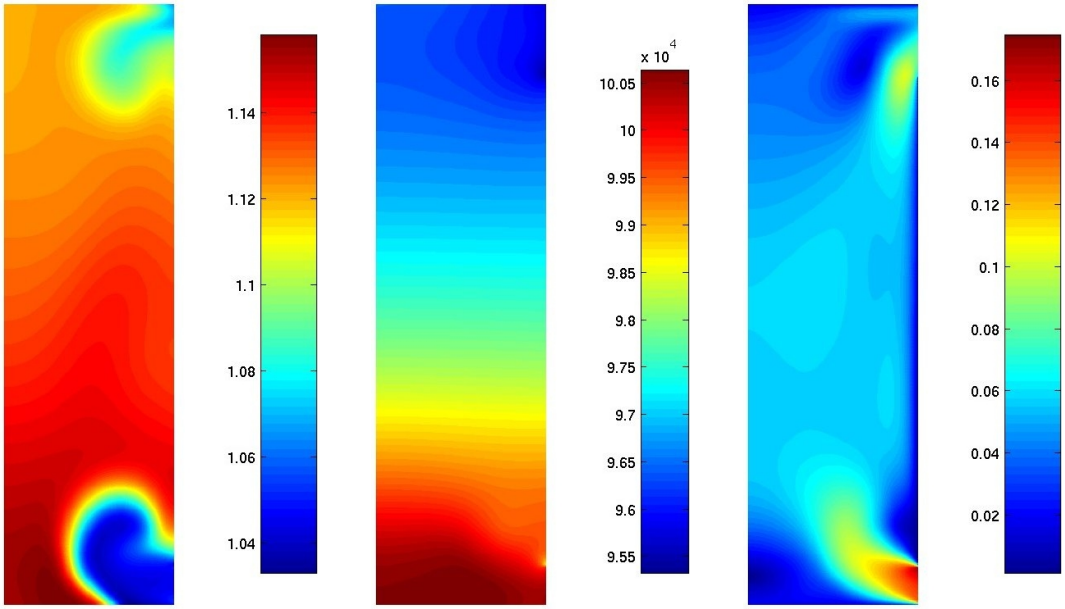

(a) Density [kg/m^3] (b) Pressure [Pa] (c) Mach number

Figure 19. State of the flow at pass half of the exhaust period (321 CAD) in the axisymmetric opposed-piston engine test computed with the UP strategy.

17. Nigro N, Storti M, Idelsohn S, Tezduyar T. Physics based GMRES preconditioner for compressible and incompressible Navier-Stokes equations. *Computer Methods in Applied Mechanics and Engineering* 1998; **154**:203–228.
18. Hirsch Ch. *Numerical Computation of Internal and External Flows. Volume 2: Computational Methods for Inviscid and Viscous Flows.* John Wiley & Sons, 1990.
19. Merkle CL. Computation of flows with arbitrary equations of state. *AIAA Journal* 1998; **36**:515–521.
20. Donea J, Giuliani S, Halleux JP. An arbitrary, Lagrangian-Eulerian finite element method for transient dynamic fluid-structure interactions. *SIAM Journal on Scientific Computing* 1982; **33**:689–700.
21. Eaton JW. *GNU Octave*. Copyright © 1998-2010. University of Wisconsin, Department of Chemical Engineering, Madison WI 53719. http://www.gnu.org/software/octave
22. Hughes T, Mallet M. A new finite element method for CFD: III. The generalized streamline operator for multidimensional advection-diffusion systems. *Computer Methods in Applied Mechanics and Engineering* 1986; **58**:305–328.
23. Le Beau G, Ray S, Tezduyar T. SUPG finite element computation of compressible flows with the entropy and conservation variables formulations. *Computer Methods in Applied Mechanics and Engineering* 1993; **104**:27–42.
24. Aliabadi S, Ray S, Tezduyar T. SUPG finite element computation of viscous compressible flows based on the conservation and entropy variables formulations. *Computational Mechanics* 1992; **11**:300–312.
25. Storti MA, Nigro NM, Paz RR, Dalcín LD. Dynamic boundary conditions in computational fluid dynamics. *Computer Methods in Applied Mechanics and Engineering* 2008; **197**:1219–1232.
26. Ansdale RF. *The Wankel RC Engine Desing and Performance*. Iliffe Books, London, 1968.
27. Toth JA. *Motor Rotativo de Combustión a Volumen Constante (MRCVC)*. Patent Res. N° AR004806B1, Rec. N° P 19960105411, 2004.
28. Brooks A, Hughes T. Streamline upwind Petrov-Galerkin formulations for convection dominated flows with particular emphasis on the incompressible Navier-Stokes equations. *Computer Methods in Applied Mechanics and Engineering* 1982; **32**:199–259 .

29. Tezduyar T, Mittal S, Ray S, Shih R. Incompressible flow computations with stabilized bilinear and linear equal order interpolation velocity-pressure elements. *Computer Methods in Applied Mechanics and Engineering* 1992; **95**:221–242.
30. Ghia U, Ghia K, Shin C. High-Re solutions for incompressible flow using the Navier-Stokes equations and a multigrid method. *Journal of Computational Physics* 1982; **48**:387–411.
31. Pedley T, Stephanoff K. Flow along a channel with a time-dependent indentation in one wall: the generation of vorticity waves. *Journal of Fluid Mechanics* 1985; **160**:337–367.
32. Ralph M, Pedley T. Flow in a channel with a moving indentation. *Journal of Fluid Mechanics* 1988; **190**:87–112.
33. Demirdžić I, Perić M. Finite volume method for prediction of fluid flow in arbitrarily shaped domains with moving boundaries. *International Journal for Numerical Methods in Fluids* 1990; **10**:771–790.
34. López E, Nigro N, Storti M, Toth J. A minimal element distortion strategy for computational mesh dynamics. *International Journal for Numerical Methods in Engineering* 2007; **69**:1898–1929.
35. Amsden AA. *KIVA-3: A KIVA program with block-structured mesh for complex geometries.* Technical report, Los Alamos, New Nexico, 1993.
36. Smagorinsky J. General circulation experiments with the primitive equation: I the basic experiment. *Monthly Weather Review* 1963; **91**:216-211.
37. Wilcox DC. *Turbulence Modeling for CFD.* D C W Industries, 2 edition, 2002.